



## Asymmetric Thermal and Water Vapor Transport of Polyester Spacer and Cotton Nonwoven Fabric Assembly

Qing Chen, Dahua Shou, Chao Sun, Bailu Fu, Rong Zheng & Jintu Fan

To cite this article: Qing Chen, Dahua Shou, Chao Sun, Bailu Fu, Rong Zheng & Jintu Fan (2023) Asymmetric Thermal and Water Vapor Transport of Polyester Spacer and Cotton Nonwoven Fabric Assembly, Journal of Natural Fibers, 20:1, 2152148, DOI: [10.1080/15440478.2022.2152148](https://doi.org/10.1080/15440478.2022.2152148)

To link to this article: <https://doi.org/10.1080/15440478.2022.2152148>



© 2022 The Author(s). Published with license by Taylor & Francis Group, LLC.



Published online: 28 Dec 2022.



Submit your article to this journal [↗](#)



Article views: 864



View related articles [↗](#)



View Crossmark data [↗](#)

# Asymmetric Thermal and Water Vapor Transport of Polyester Spacer and Cotton Nonwoven Fabric Assembly

Qing Chen<sup>a</sup>, Dahua Shou<sup>b</sup>, Chao Sun<sup>c</sup>, Bailu Fu<sup>a</sup>, Rong Zheng<sup>a</sup>, and Jintu Fan<sup>b</sup>

<sup>a</sup>Shanghai International Fashion Innovation Center, Donghua University, Shanghai, China; <sup>b</sup>The School of Fashion and Textiles, The HongKong Polytechnic University, Hongkong, China; <sup>c</sup>The School of Art and Design, China Women's University, Beijing, China

## ABSTRACT

Spacer fabric is often used in cushions, footwear, filter material, and other products because of its high air permeability and three-dimensional (3D) structure. However, for practical applications, it is typically combined with other materials. We investigated the thermal properties and water vapor permeability of assembly-combined thicker spacer (16 mm) and various cotton nonwoven fabrics. The assembly-combined lightest nonwoven (30 g/m<sup>2</sup>) and spacer fabric exhibited the highest thermal resistance, increasing by 66.62% compared with the bare spacer fabric; however, no significant difference was observed when combined with the heaviest woven fabric (60 g/m<sup>2</sup>). Furthermore, the fabric arrangement during assembly could affect the heat and moisture-transfer efficiencies. The assembly-combined lightest nonwoven (30 g/m<sup>2</sup>) and spacer fabric under the upward test condition exhibited the highest thermal resistance, highest Clo, lowest heat transfer coefficient, highest insulation ratio, and lowest evaporation resistance among all assemblies. Higher thermal resistance and lower evaporative resistance could benefit physiological comfort. However, the assembly-combined heaviest nonwoven and spacer fabric under the downward test condition exhibited similar thermal resistance to the spacer fabric and the highest evaporation resistance. The asymmetric heat- and moisture-transfer properties of a porous assembly can contribute toward developing new materials for applications in other engineering fields.

## 摘要

间隔织物由于其高透气性和三维 (3D) 结构, 经常用于垫子、鞋类、过滤材料和其他产品。然而, 对于实际应用, 它通常与其他材料结合。我们研究了组合较厚垫片 (16 mm) 和各种棉质非织造织物的热性能和水蒸气渗透性。组合最轻的非织造布 (30 g/m<sup>2</sup>) 和间隔织物的组件表现出最高的热阻, 与裸间隔织物相比增加了 66.62%; 然而, 当与最重的机织物 (60 g/m<sup>2</sup>) 组合时, 没有观察到显著差异。此外, 组装过程中的织物布置可能会影响热传递和水分传递效率。在向上测试条件下, 组合最轻的非织造布 (30 g/m<sup>2</sup>) 和间隔织物的组件在所有组件中表现出最高的热阻、最高的 Clo、最低的传热系数、最高的绝缘比和最低的蒸发阻力。较高的热阻和较低的蒸发阻力有利于生理舒适。然而, 在向下测试条件下, 组合最重的非织造布和间隔织物的组件表现出与间隔织物相似的热阻和最高的蒸发阻力。多孔组件的非对称传热和水分传递特性有助于开发其他工程领域应用的新材料。

## KEYWORDS



Thermal resistance; water vapor resistance; spacer; nonwoven; asymmetric

## 关键词

热阻; 抗水汽性; 垫片; 非织造的; 不对称

## Introduction

Spacer fabric is widely used in filtration, mattresses (Onal and Yildirim 2012), cushions (Arumugam et al. 2018), shoes (Lo et al. 2018), and bras (Yip and Ng 2009) because of its excellent support and

**CONTACT** Dahua Shou  [dahua.shou@polyu.edu.hk](mailto:dahua.shou@polyu.edu.hk)  The school of Fashion and TextilesThe Institute of Textiles and Clothing The HongKong Polytechnic University, Hongkong China

© 2022 The Author(s). Published with license by Taylor & Francis Group, LLC.

This is an Open Access article distributed under the terms of the Creative Commons Attribution License (<http://creativecommons.org/licenses/by/4.0/>), which permits unrestricted use, distribution, and reproduction in any medium, provided the original work is properly cited.

recovery with high water evaporation. The spacer fabric has a three-dimensional (3D) structure, a higher thickness, and a lighter weight compared with other traditional materials; therefore, many studies have been conducted to investigate its mechanical properties – compression (Ozer, Yuksel, and Korkmaz 2020), tensile (Ghorbani et al. 2020), and transmissibility (Krumm, Schwanitz, and Odenwald 2020)—for developing composites. Spacer fabric was used recently to develop a composite for solar thermal energy harvesting (Jia et al. 2018), triboelectric nanogenerator (Zhu et al. 2016), and solar steam generation (Wang et al. 2019) because of its unique structure.

Many studies have investigated the effect of fiber type on the thermal and water vapor transmission properties of spacer. The thicker, heavier flat-knitted spacer ( $1,291\text{--}1,642.2\text{ g/m}^2$ ,  $8.2\text{--}11.3\text{ mm}$ ) was produced by polyester and Coolmax® (Gozde 2017). The Coolmax® spacer has a higher air permeability, water vapor permeability index, and thermal resistance ( $0.1691\text{ m}^2\cdot\text{K/W}$ ). The effects of fiber type on the thermal properties of the circular knitted spacer fabrics ( $437\text{--}505\text{ g/m}^2$ ,  $3.66\text{--}3.97\text{ mm}$ ) made from functional fibers (i.e., Outlast® and Coolmax®), polyester, and cotton were studied (Onal and Yildirim 2012). The thermal resistance of these fabrics was in the range of  $0.065\text{--}0.073\text{ m}^2\cdot\text{K/W}$ . Circular knitted spacer ( $443\text{--}695\text{ g/m}^2$ ,  $2.62\text{--}4.4\text{ mm}$ ) with polypropylene or elastic yarn on one surface and with polyester monofilament or multifilament in the middle were developed (Veerakumar et al. 2017). The water vapor resistance (Ret) of the developed fabrics was approximately  $6.34\text{--}18.61\text{ m}^2\cdot\text{K/W}$ .

Furthermore, the effects of different knitted or 3D-printed structures on thermal properties have been studied. A circular knitted spacer with a mass ranging from  $315.8$  to  $393.6\text{ g/m}^2$  and a thickness ranging from  $2.265$  to  $3.523\text{ mm}$  had a thermal resistance ranging from  $0.0518$  to  $0.0695\text{ m}^2\cdot\text{K/W}$  (Ertekin and Marmarali 2011). Compared with traditional warp-knitted spacer fabric, the flat-knitted spacer fabric ( $487.3\text{--}1182.3\text{ g/m}^2$ ,  $3.72\text{--}7.22\text{ mm}$ ) was more suitable for comfortable apparel with a thermal resistance of approximately  $0.0793\text{--}0.1343\text{ m}^2\cdot\text{K/W}$  (Chen et al. 2018). The water vapor permeability is highly influenced by the porosity of the spacer fabrics (Rajan et al. 2016).

In this study, the permeability of fabrics depended on the porosity, the pore and filament radii, and the air gap between the layers of the fabric. The high volume of voids within the fabrics determines the holding property and permeability of water. A 3D-printed spacer material with different surface pore sizes ( $6$  and  $9\text{ mm}$ ) and thicknesses ( $9\text{--}23\text{ mm}$ ) have been developed using thermoplastic polyurethane (Eom, Lee, and Lee 2019). Under the heating condition, the material with large pores and high thickness had higher thermal insulation, while under the no heating condition, the air-gap thickness dominated the thermal insulation.

The thermal characteristics of the spacer are also crucial for its wide application over sponge or foam. Many treatments or finishing methods have been applied to improve its thermal properties. Rajan et al. used argon plasma treatment to improve the thermo-physiological comfort of the spacer used for a shoe insole. The  $3\text{-mm}$  thickness of the polyester spacer fabric has superior response and comfort properties to the  $2\text{-}$  and  $4\text{-mm}$ -thick spacer fabrics after plasma treatment (Rajan and Sundaresan 2020). A three-layered fabric system was constructed to improve thermal properties and prevent air convection through spacer fabric; the fabric system consisted of a 3D-knitted polyester spacer fabric in the middle and was integrated by two layers of knitted cotton fabrics impregnated with silica at both sides (Ziaei and Ghane 2013). This multilayer construction that was integrated with ceramic powder had a significant effect on increasing the thermal resistance property compared with the untreated spacer fabric. The thermal resistance of two-layer fabric ensembles featuring thick, open-structure mid-layer insulation and a thin shell-layer can be markedly increased by metalizing both layers (Morrissey and Rossi 2015). Metalized mid- and shell-layers increased the thermal resistance of the fabric assemblies, and the increase in thermal resistance was highest when the thickness and optical porosity of the middle layer were sufficiently high.

Furthermore, multilayered systems have been explored to enhance comfort. In a clothing system, the thermal and moisture vapor transmission properties of three-layer fabric ensembles—(1) an inner layer composed of raised fabric, needle punched fabric, air-bonded fabric, spun-bonded sandwiched nonwoven fabric and spacer fabric, (2) a middle layer composed of woven coated rubber, polyester polymer, and poly tetra fluoroethylene (PTFE) fabrics, and (3) an outer layer composed of cotton

woven fabric – were investigated (Das 2012). Lower moisture vapor transmission may cause condensation within the clothing system. The layer arrangement of a multiplayer clothing system can alter its heat- and moisture-transfer properties (Yoo and Kim 2008). An appropriate layer arrangement, layer design, and material selection should be considered to manipulate the performance of cold-weather ensembles for heat- and moisture-transfer properties, especially to address condensation problems. The effects of fabrics on the thermal and evaporation resistance of the ensembles in personal protective equipment were evaluated using a sweating guard hotplate (Xu et al. 2019). The fabrics contributed 10% of the thermal resistance and 14% of the evaporative resistance of these 14 multilayer ensembles.

A series of multilayered fabric assemblies have been produced with different combinations of fabric layers (e.g., plain woven, nonwoven wadding, warp-knitted spacer fabric, weft-knitted breathable coated, and weft-knitted aluminum coated) and air gaps of different thicknesses between the fabric layers (Das et al. 2012). In the absence of an air gap between the fabric layers, the thermal transmission of the clothing assembly was governed primarily by the thermal resistance of the component fabric layer. The thermal resistance of all the fabric assemblies at any given air-layer thickness was highest under the non-convective mode of heat transmission, followed by the natural convection mode. Moreover, the forced convection mode exhibited the least thermal resistance.

The layer array effects of the multilayer cold-weather clothing ensembles on heat and moisture transfer and condensation profiles were examined using a human-clothing-environment simulator (Yoo and Kim 2008). The underwear was polyester knit. The first to third layers were polyester fleece for the inner layer, PTFE for the middle layer, and laminated waterproof breathable fabric for the outer layer. Without altering materials, the layer arrangement influenced the condensation profiles and the heat and water vapor permeability of the clothing ensembles.

The mechanical attachment of a lightweight wool web (a mass of 50–100 g/m<sup>2</sup>) to one surface of a highly permeable, warp-knitted spacer fabric (thicknesses of 9.2 and 2.4 mm) using hydroentanglement noticeably decreased the transverse thermal conductivity of the resultant fabric (Mao and Russell 2007). Multilayer clothing assemblies consisting of fibrous battings and reflective nano-fibrous thin layers for cold protective clothing can improve thermal insulation (Sun et al. 2013). The differences in thermal sensation magnitudes can be caused by the thermal properties of different materials (Sinclair, 2014 and Tang, Wu, and Fan 2020). That study examined thin spacer fabric (2.62–11.3 mm) with low thermal resistance (0.0518–0.1691 m<sup>2</sup> · K/W).

Moreover, different fabric and fabric arrangements were explored to improve the thermal insulation in multilayered garment systems. In a previous study (Chen et al. 2021), if the spacer fabric had a mesh structure on one side and a plain structure on the other, the water vapor permeability differed when testing the sample under two conditions (one was placed plain side up, the other was placed on the mesh side up). The arrangement of the surface fabric on spacer fabric impacted the evaporation resistance significantly. However, no studies to our knowledge have examined the effect of the arrangement of surface fabric on spacer fabric on thermal and moisture transportation to improve thermal and evaporation efficiency.

The spacer was included with other fabrics because it is a supporting shell with unsmooth surfaces. In real-world applications of mattresses, cushions, or protective clothing, spacer will be combined with other lining or cover fabrics (e.g., woven fabrics, knitted fabrics, or nonwoven fabrics with different fiber types). For improved touch with the skin, cotton was used as cover for home textiles or underwear applications. For example, babies aged 1–6 months cannot turn over by themselves. In hot weather or wet urine, bacteria grow easily, affecting the baby's health. Therefore, the cushion produced by spacer fabric can be used, and the upper and lower surfaces can be covered with nonwoven fabric. This type of cushion is breathable and can absorb moisture to keep the body dry.

In this study, the thermal and water vapor transmission properties of a polyester spacer with relatively lighter mass and higher thickness (742 g/m<sup>2</sup>, 16 mm) and a cotton nonwoven (30–60 g/m<sup>2</sup>, 0.19–0.25 mm) assembly are reported. Asymmetric transportation of heat and moisture occurred depending on the arrangement of nonwoven particles on the top or bottom surface of the spacer. This

observation establishes a foundation for developing a system with high thermal retention, high moisture evaporation, substantial energy savings, and improved thermal comfort.

## Materials and methods

### Sample preparation

The polyester warp-knitted spacer fabric has a fabric weight of 742.02 g/m<sup>2</sup> and a thickness of 16 mm. The cotton nonwoven fabrics had fabric weights of 30, 40, 50, and 60 g/m<sup>2</sup> and thicknesses of 0.19, 0.21, 0.23, and 0.25 mm. Figure 1 demonstrates the two surfaces and the cross-section of the spacer.

### Aperture analyzer for nonwoven fabrics

A porous materials instrument (PMI CFP-1100AI) was used to evaluate the pore size of the nonwoven fabrics. The smallest, medium, and largest detected pore diameters were directly obtained from the instrument.

### Air permeability for nonwoven fabrics

Air permeability was determined by the difference between the pressures on both the ends of the fabric and the airflow rate through the fabric. According to the China standard of GB/T 5453-1997 (Textiles – determination of the permeability of fabrics to air, equal to ISO 9237:1995 Textiles – determination of permeability of fabrics to air), YG(B)461E was used to measure the air permeability of the fabrics. It was measured at the pressure drop of 100 Pa on both sides of the fabric. The sample size is 10 × 10 cm, the test area is 20 cm<sup>2</sup>, and the pressure drop is 100 Pa. The results were obtained directly from the apparatus. Only nonwoven fabrics were tested because others were too thick to be clamped by the instrument. The air permeability was calculated as follows:

$$R = \frac{qV}{A} \times 167$$

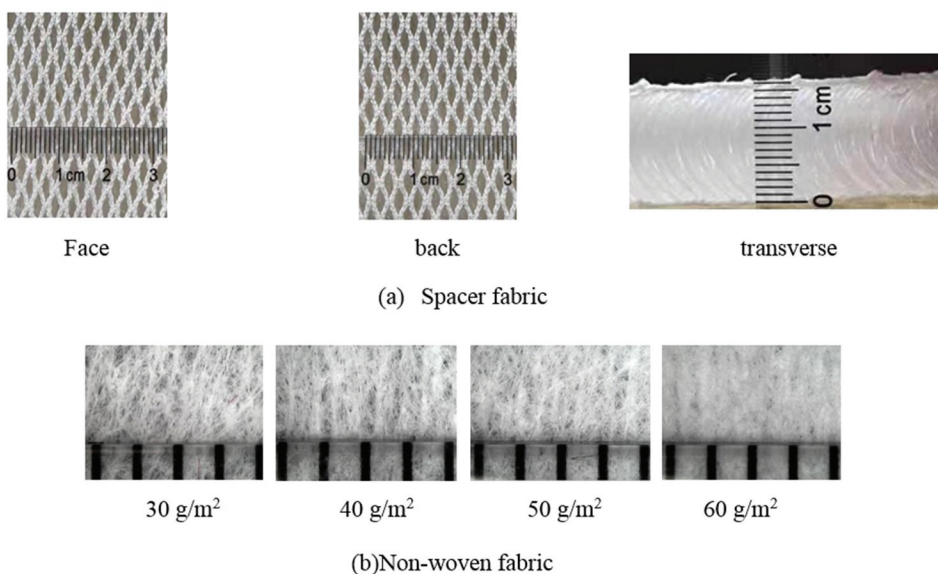
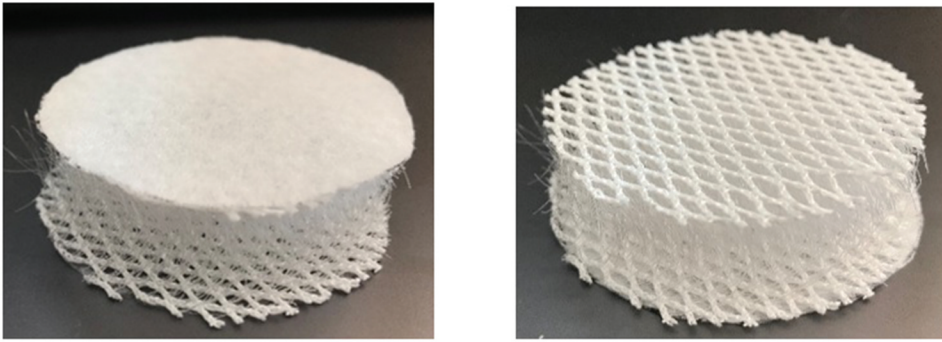


**Figure 1.** The pictures of different views of spacer fabric and non-woven fabric.





(a) non-woven at the top of a spacer      (b) non-woven at the bottom of a spacer

**Figure 2.** Cotton non-woven – polyester spacer assemblies during the analysis using a hot plate instrument.

where  $qv$  is the arithmetic mean flow rate of air (in cubic decimeters per minute, L/min),  $A$  is the area of fabric under test (in square centimeters,  $\text{cm}^2$ ), and 167 is the conversion factor from cubic decimeter (or liters) per minute per square centimeter to millimeters per second.

### **Thermal and evaporation resistance**

According to ASTM F1868 (standard testing method for thermal and evaporation resistance of clothing using a sweating hot plate), the  $50 \times 50$  cm samples were tested on YG 606 G-II, a hot plate instrument. The temperature of the hot plate was maintained at approximately  $36^\circ\text{C}$ , and the temperature of the testing chamber was maintained at approximately  $20^\circ\text{C}$ . The thermal resistance,  $\text{Clo}$  ( $1 \text{ Clo} = 0.155 \text{ m}^2 \cdot \text{K}/\text{W}$ ), heat transfer coefficient, thermal insulation ratio, evaporation resistance, and water vapor transmission rate were displayed directly on the instrument's screen. The cotton nonwoven fabric, polyester spacer fabric, and cotton non-woven-polyester spacer assembly (upward or downward depicted in Figure 2) were tested. The thermal- and moisture-transmission efficiencies as a function of the combination method were measured using two approaches: cotton nonwoven was placed below or above the polyester spacer.

The equations are defined as follows:

$$R_{ct} = \frac{(T_m - T_a) \times A}{H - H_c} - R_{ct0}$$

$$R_{et} = \frac{(P_s - P_a) \times A}{H - H_e} - R_{et0}$$

$$\text{Clo} = \frac{R_{ct}}{0.155}$$

$T_m$ —temperature of hot plate

$T_a$ —temperature of air in chamber

$H$ —heat consumption of hot plate and fabric

$H_c$ —heat consumption of hot plate

$A$ —area of testing plate

$R_{ct0}$ —thermal resistance of hot plate

$P_s$ —moisture pressure in chamber at  $T_a$

$P_a$ —saturated moisture pressure in chamber at  $T_m$

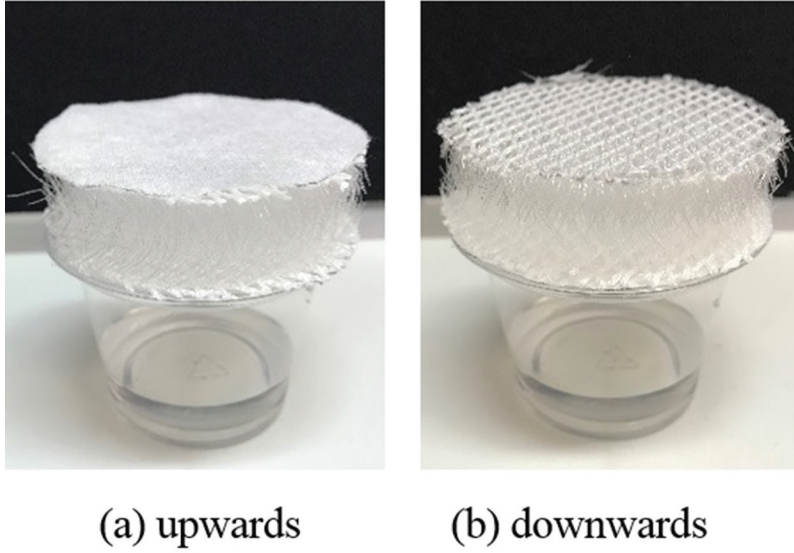


**Figure 3.** The illustration of unsealed and sealed samples in water vapor permeability test.

### ***Water vapor permeability***

Water vapor permeability was measured according to the China standard GB/T 127,042–2009 (the water vapor permeability of textile measurement method). Fabric samples and water were conditioned for at least 1 day in an environment with a temperature of  $20 \pm 2^\circ\text{C}$  and relative humidity of  $65 \pm 2\%$ . Ten milliliters of water was placed into the cup, each sample was placed on the top of the cup, and each cup was sealed with tape. The cup and fabric were weighted as an original assembly weight ( $M_1$ ). After 24 h, the total weight of the cup and fabric were measured ( $M_2$ ). Three pieces of each sample were tested. The average values are calculated using Equation 1.  $A$  is the fabric sample-tested area, and  $t$  is 24 h. All fabrics were also tested using an approach similar to those depicted in Figure 3. According to the water loss of every square meter of fabric after 1 day, the greater the value, the higher the water vapor permeability. Cotton nonwoven fabric, polyester spacer fabric, and cotton nonwoven polyester spacer assembly were tested individually.

$$WVP = \frac{M_2 - M_1}{A \cdot t} \quad (\text{g/m}^2 \cdot 24\text{h}) \quad (1)$$

### ***The regression model***

The linear regression models were estimated using SPSS software.

## **Results and discussion**

### ***Pore size and air permeability of nonwoven fabrics***

The results of pore sizes of the nonwoven fabrics and air permeability are depicted in Figures 4 (a) and (b). There were similar declining trends of pore size and air permeability from 30 to 60  $\text{g/m}^2$  of the nonwoven fabrics because the permeability of fibrous porous media depends significantly on the maximum pore scale (Shou et al. 2014; Shou, Fan, and Ding 2010).

Based on the testing results, a linear regression equation is established between them as follows:

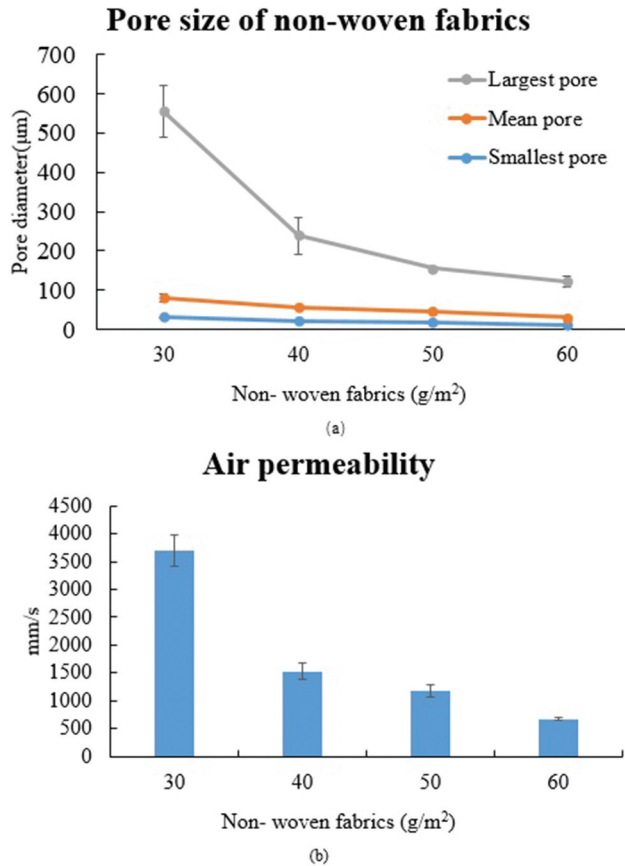


**Figure 4.** Pore size, air permeability, and water vapor permeability of non-woven fabrics.

$Y$  (air permeability) =  $-367.946 - 59.105 \times \text{smallest pore diameters} + 65.090 \times \text{mean pore diameters} + 5.748 \times \text{largest pore diameters}$  (adjust R square = 1). (1)

The smallest pore diameters ranged from 31.56 to 11.7  $\mu\text{m}$ , the mean pore diameters ranged from 49.39 to 18.52  $\mu\text{m}$ , and the largest pore diameters ranged from 473.75 to 91.36  $\mu\text{m}$ . Air permeability ranged from 3699.13 to 671.1 mm/s. As the pore size decreased, the air permeability also declined. The largest decrease in pore size percentage was approximately 61.69% (442  $\mu\text{m}$  decrease), causing an 81.858% reduction (3028.03 mm/s) in air permeability.

### **Thermal properties of polyester warp-knitted spacer fabric and assembly (nonwoven + spacer)**

#### **Thermal resistance**

As depicted in Figure 5(a), the thermal resistance of the cotton nonwoven fabrics decreased from the lightest sample ( $0.042 \text{ m}^2 \cdot \text{K/W}$  for 30 g/m<sup>2</sup>) to the heaviest sample ( $0.024 \text{ m}^2 \cdot \text{K/W}$  for 60 g/m<sup>2</sup>) because of the dense structure and small pore size of the fabric. There was a reduction of 42.024% in the thermal resistance. The thermal properties were determined by fiber type, fiber arrangement, and air volume in the fabrics. In a thin fabric, there is predominantly heat conduction. The fiber substance had little influence on  $R_{\text{ct}}$ , while the bulk density of the nonwoven fabric is essential to the thermal resistance (Sinclair 2014). Materials with large pores had higher thermal resistance (Eom, Lee, and Lee 2019). With the increase in the bulk densities of nonwoven fabrics (1,578, 1,904, 2,173, and 2,400 g/cm<sup>3</sup>), decreases in pore size and air volumes were observed. A smaller air volume entrapped in the



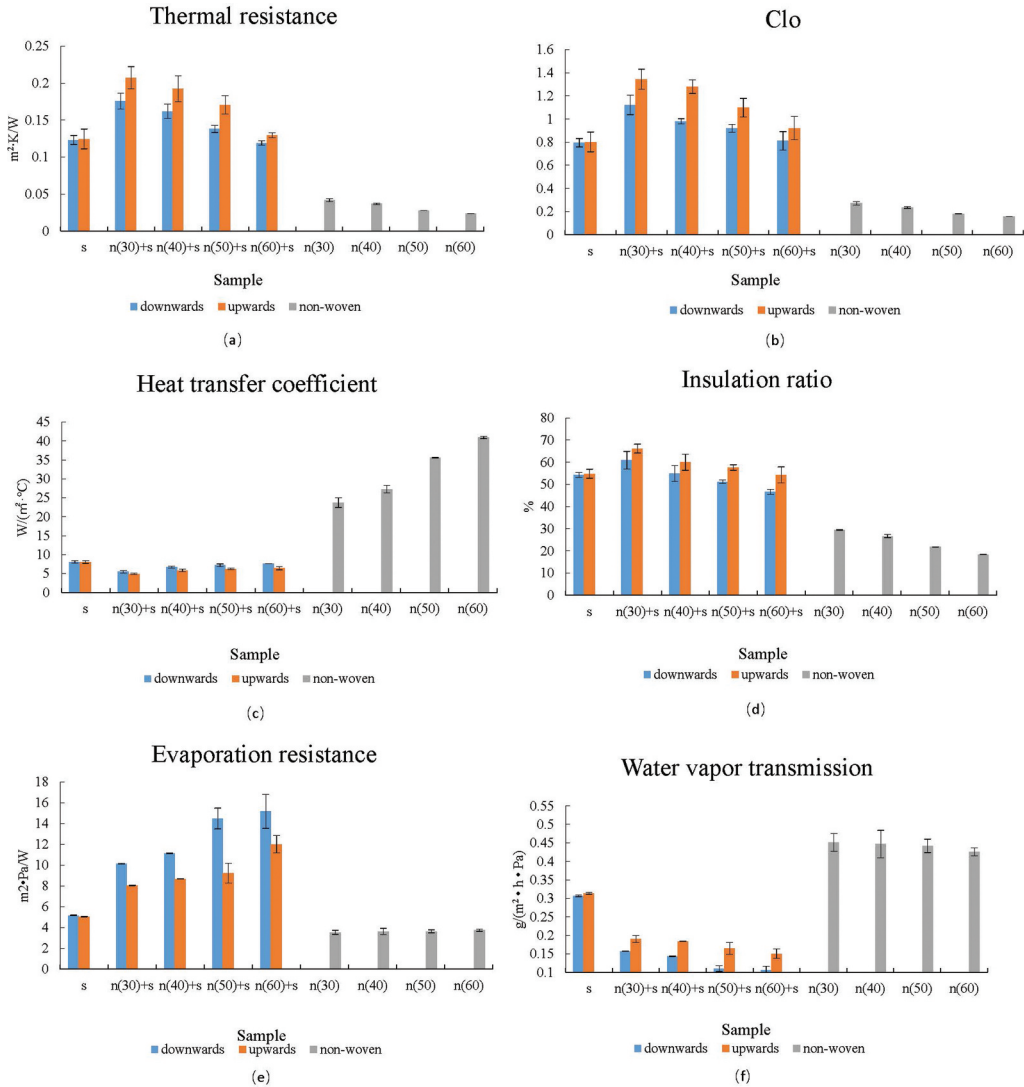


**Figure 5.** Thermal resistances(a) and Clo(b) of spacer, assembly, and non-woven fabric. (Spacer fabric and the assembly constructed with  $30 \text{ g/m}^2/40 \text{ g/m}^2/50 \text{ g/m}^2/60 \text{ g/m}^2$  of non-woven and spacer fabric are represented by "s" and "n(30/40/50/60)+s," respectively.). Heat transfer coefficient(c) and insulation ratio(d) of spacer, assembly, and non-woven fabric. (Spacer fabric and the assembly constructed with  $30 \text{ g/m}^2/40 \text{ g/m}^2/50 \text{ g/m}^2/60 \text{ g/m}^2$  of non-woven and spacer fabric are represented by "s" and "n(30/40/50/60)+s," respectively.). Evaporation resistance(e) and water vapor transmission(f) of spacer, assembly, and non-woven fabric. (Spacer fabric and the assembly constructed with  $30 \text{ g/m}^2/40 \text{ g/m}^2/50 \text{ g/m}^2/60 \text{ g/m}^2$  of non-woven and spacer fabric are represented by "s" and "n(30/40/50/60)+s," respectively.).

material indicated less insulating power, resulting in greater heat transfer via conduction and lower thermal resistance of the textile material. In this case, the higher mass and thickness of the nonwoven fabric resulted in a lower thermal resistance than that of lower mass and thickness.

Heat conduction, heat convection, and heat radiation are present in porous and thick fabric ( $>10 \text{ mm}$ ). Hence, the thermal resistance of the spacer fabric ( $0.123$  and  $0.124 \text{ m}^2 \cdot K/W$ ) was the lowest compared with the nonwoven spacer assembly because the spacer fabric has mesh on both surfaces where the heat convection was dominant. After the large pores on the surface of the spacer were covered by the nonwoven fabrics, the more the still air trapped during assembly could diminish the heat transfer by convection and increase the heat transfer by conduction. The still air had a much

lower thermal conductivity (0.023–0.026 W/m·°C) than cotton fiber (approximately 0.071 W/m·°C) and polyester fiber (approximately 0.084 W/m·°C).

The thermal resistance of the assembly decreased with the increasing mass of the nonwoven fabric regardless of the test condition (upward or downward). There was no difference when the spacer was tested downward or upward because of the same structure on both surfaces. However, when the nonwoven fabric was placed far away from the hot plate and on the top of the spacer, it had a higher thermal resistance than when near the hotplate and at the bottom of the spacer. The thermal resistance is calculated as  $R = \frac{T}{Q}$ .  $R$  is the thermal resistance of testing samples,  $Q$  is the heat required to maintain the temperature of the hotplate at 36°C, and  $\Delta T$  is the difference in temperature at the top or bottom surface, where it is 16°C. When the nonwoven fabric was placed under the spacer, the nonwoven surface was in direct contact with the hot plate, which could increase the conductive heat transfer and airflow in the spacer because of the top mesh surface.

When the nonwoven fabric was placed above the spacer, it decreased the assembly contact area with the hot plate because of the mesh surface of the spacer, weakening the conductive heat transfer because less contact with the hot plate could result in a lower rate of the heat transfer by conduction (Morrissey and Rossi 2015). In this arrangement, more still air could be trapped between the two surfaces of the spacer because of the large thickness (16 mm) of the assembly and the nonwoven fabric at the top surface of the meshed spacer. The air gap can increase the insulation efficiency; however, the construction surface also affects the thermal transmission (Rajan and Sundaresan 2020). This construction feature of assembly could help maintain the hotplate at a constant temperature, consuming less heat energy. In real-world wearing conditions, this garment could generate different temperatures on the top and bottom surfaces to drive the heat transfer through the cross-section asymmetrically. This structure could result in a low-temperature gradient difference and decrease heat loss in the body.

Compared to the assembly with spacer, the maximum enhancement reached 66.62% when 30-g/m<sup>2</sup> nonwoven was attached to the assembly upward, while the minimum was only 3.32% when 60-g/m<sup>2</sup> nonwoven was attached to the assembly downward, where no difference was found. In contrast, the assembly with the lightest nonwoven fabric had the highest thermal resistance, likely because the effective diffusivity depends on the ratio of the minimum and maximum pore size (Mao and Russell 2008). Furthermore, the differences between the values in upward and downward testing methods were 18%, 18.6%, 23.45%, and 8.81%, which decreases with an increase in the mass of the nonwoven fabrics. These results reveal that the proper pore size of the top layer in the assembly could enlarge the thermal resistance of the assembly in a no-wind condition. A smaller air volume entrapped in the nonwoven fabric resulted in less insulating power, and a higher heat transfer by conduction resulted in less thermal resistance of the nonwoven fabrics (Sinclair 2014).

Furthermore, the thermal resistance of the assemblies n(30)+s, n(40)+s, and n(50)+s under the upward test condition (0.2074, 0.1925, and 0.1705 m<sup>2</sup>·K/W, respectively) were higher than the sum of the individual spacer and the nonwoven fabric (0.1665, 0.1615, and 0.1525 W/m·°C, respectively). However, the thermal resistance of the assembly n(30)+s under the downward test condition was only higher than the sum of those of the individual spacer and 30 g/m<sup>2</sup> nonwoven fabric, while others were lower than that of the spacer and nonwoven. These results confirmed that the arrangement of individual fabrics during assembly could significantly affect the thermal properties. A random combination of different fabrics may not effectively improve the performance in contrast to increasing the total weight of the assembly.

The regression model of the thermal resistance was estimated by mass and mean pore size of the nonwoven fabric, as defined in Equations 2 and 3. The adjusted R square values reached 0.999 and 0.861 when the nonwoven fabric was placed under and above the spacer.

$$\text{Thermal resistance of assembly}_{\text{down}} = 0.304 - 0.003 \times \text{mass of non-woven} - 0.892 \times \text{mean pore size, Adjusted } R^2 = 0.999 \quad (2)$$

$$\begin{aligned} \text{Thermal resistance of assembly}_{\text{up}} &= 0.356 - 0.003 \times \text{mass of non woven} - 0.866 \\ &\times \text{mean pore size, Adjusted } R^2 = 0.861 \end{aligned} \quad (3)$$

### Clo

“Clo” is the approximate insulation required to keep a resting person (producing heat at the rate of 58 W/m<sup>2</sup>) comfortable at an ambient temperature of 21°C and air movement of 0.1 m/s (approximately the insulation value of typical indoor clothing) (Veerakumar et al. 2017).

As depicted in Figure 5(b), the values of Clo had a trend similar to the thermal resistance (Figure 4), which was because Clo depended on thermal resistance, i.e.,  $\text{Clo} = \frac{\text{thermal resistance}(\frac{\text{m}^2\text{K}}{\text{W}})}{0.155(\frac{\text{m}^2\text{K}}{\text{W}})}$ .

After comparing the assembly (n(30)+s upward) with the spacer and nonwoven fabric separately, there was a 67% increase over the spacer and a 394% increase over the nonwoven (30 g/m<sup>2</sup>). The Clo value of nonwoven fabrics also decreased from 0.272 of 30 g/m<sup>2</sup> nonwoven to 0.157 of 60 g/m<sup>2</sup> nonwoven, with a 42.173% reduction because the 30-g/m<sup>2</sup> nonwoven fabric has the largest mean pore size (49.39 μm) among these four nonwoven fabrics.

The Clo values of the normal fabrics are generally less than 1. However, the Clo value of the assembly-combined spacer and nonwoven fabrics reached 1.345. Hence, the nonwoven fabric on the surface of the spacer has a significant impact on the heat transmission of the assembly. This method could be effective for achieving higher Clo values by combining the nonwoven fabrics at the top surface of the spacer. The estimated equations of the Clo values are defined in Equations 4 and 5 with adjusted R square values at 1 and 0.964, corresponding to the two test conditions.

$$\begin{aligned} \text{Clo of assembly}_{\text{down}} &= 0.876 - 0.003 \times \text{mass of non - woven} + 6.953 \\ &\times \text{mean pore size, Adjusted } R^2 = 1 \end{aligned} \quad (4)$$

$$\begin{aligned} \text{Clo of assembly}_{\text{up}} &= 2.650 - 0.025 \times \text{mass of non woven} - 10.937 \\ &\times \text{mean pore size, Adjusted } R^2 = 0.964 \end{aligned} \quad (5)$$

### Heat transfer coefficient

As depicted in Figure 5(c), the values of heat transfer coefficient have a trend similar to that of thermal resistance (Figure 5(a)) because the heat transfer coefficient =  $\frac{1}{\text{thermal resistance}}$ . The heat transfer coefficient of the nonwoven fabrics increased from 23.775 to 40.945 W/(m<sup>2</sup> · k), with an increase of 72.219% caused by the decrease in the mean pore size of nonwoven from 49.39 to 18.52 μm. The spacer fabric had a heat transfer coefficient of approximately 8.1 W/(m<sup>2</sup> °C) because of its high thickness (16 mm) compared with the nonwoven fabric (0.19–0.25 mm). The assembly (n (30) + s) under the upward test condition exhibited the lowest heat transfer coefficient (6.435 W/m<sup>2</sup> · k).

When the spacer is attached with thin and low-weight fabric, it can significantly reduce the heat transfer compared to the nonwoven and spacer. Furthermore, the reduction dropped significantly with the decreasing mass of the nonwoven fabric. The lowest value of the heat transfer coefficient was 4.945 W/m<sup>2</sup> · k for the assembly combined with 30-g/m<sup>2</sup> nonwoven and spacer fabrics under the upward test condition.

No difference was observed when the spacer was tested for two approaches (downward or upward) because of the same mesh surface of the spacer fabric. However, when the nonwoven fabric was placed far away from the hot plate, its heat-transfer ability deteriorated compared with when the testing was performed downward. Moreover, the differences between the values under the upward and downward tests were −10.41%, −12.7%, −13.38%, and −15.99% for assemblies combining spacer fabric with 30, 40, 50, and 60 g/m<sup>2</sup> nonwoven fabrics. The asymmetric heat transfer capability results from the nonwoven fabric attached at the bottom or top of the spacer.

After comparing the assembly with the spacer, the maximum decrease was 38.79% for the “n(30)+s” sample under the upward test. In contrast, the minimum decrease was 5.54% for the “n(60)+s” sample under the downward test. The estimated equations of the heat transfer coefficient values are as defined in Equations 6 and 7, with adjusted R square values of 0.908 and 0.794, corresponding to the two test conditions.

$$\text{Heat transfer coefficient of assembly}_{\text{down}} = 8.750 + 0.005 \times \text{mass of non-woven} - 66.531 \times \text{mean pore size, Adjusted } R^2 = 0.908 \quad (6)$$

$$\text{Heat transfer coefficient of assembly}_{\text{up}} = 7.703 - 0.02 \times \text{mass of non-woven} - 52.522 \times \text{mean pore size, Adjusted } R^2 = 0.794 \quad (7)$$

### Insulation ratio

The nonwoven fabric with the lightest mass had the lowest insulation ratio. When the nonwoven fabric was placed above the spacer fabric (Figure 5(d)), the insulation ratios of all the assemblies were higher than those of samples with nonwoven placed below spacer and without nonwoven fabric. There were 8.64%, 9.26%, 12.52%, and 16.34% increases for samples “n(30)+s,” “n(40)+s,” “n(50)+s,” and “n(60)+s” when comparing the two test approaches. However, when the nonwoven fabric was placed below the spacer, only the assembly with 30-g nonwoven fabric exhibited a higher insulation ratio than the spacer. This finding confirmed that the type of combination could impact the insulation ratio during the application. The thermal insulation decreased from 29.5% to 18.355% with the increasing mass of the assembly, with a 37.78% reduction in the insulation ratio.

The estimated equations of insulation ratio values are as defined in Equations 8 and 9, with the adjusted R square at 0.998 and 0.979, respectively, corresponding to the two test conditions.

$$\text{Insulation ratio of assembly}_{\text{down}} = 158.712 - 0.267 \times \text{mass of non-woven} + 204.902 \times \text{mean pore size, Adjusted } R^2 = 0.998 \quad (8)$$

$$\text{Insulation ratio of assembly}_{\text{up}} = 50.364 - 0.048 \times \text{mass of non-woven} + 334.523 \times \text{mean pore size, Adjusted } R^2 = 0.979 \quad (9)$$

### Evaporation resistance

As depicted in Figure 5(e), the evaporation resistance of nonwoven fabrics ranged from 3.54 to 3.74  $\text{m}^2 \cdot \text{Pa} / \text{W}$  with a 5.6% difference and increased with an increase in the mass of the nonwoven fabrics. The pore diameter of the nonwoven fabrics was critical to obtaining an accurate design to optimize the comfort performance [30]. Although the spacer had a much higher thickness (16 mm) than the nonwoven fabric (0.19–0.25 mm), it had an evaporation resistance of approximately 5.055–5.165  $\text{m}^2 \cdot \text{Pa} / \text{W}$ . The values of the assemblies ranged from 8.055 to 15.17  $\text{m}^2 \cdot \text{Pa} / \text{W}$  and increased with the mass of the nonwoven fabric whenever the nonwoven fabric was attached above or below the spacer.

When the assemblies were tested under the downward condition, they exhibited a higher evaporation resistance than those under the upward condition. The range of the increasing percentage of the downward test condition was approximately 20.4–36.3% when compared with values of the upward test condition. There was a concentration gradient between the top and bottom surfaces of the assembly due to a much higher thickness of the assembly and different pore sizes on the two surfaces. In contrast, cotton had higher moisture regain, increasing the difference in the concentration gradient between the two surfaces.

In the downward test condition, the evaporation resistance values of the assembly (10.125–15.17  $\text{m}^2 \cdot \text{Pa} / \text{W}$ ) were consistently higher than those of the sum of the spacer and nonwoven fabric (8.705–8.905  $\text{m}^2 \cdot \text{Pa} / \text{W}$ ). However, in the upward test condition, the assembly n(30)+s had an evaporation

resistance of  $8.055 \text{ m}^2 \cdot \text{Pa/W}$ , which was lower than that of the sum of the corresponding nonwoven fabric and spacer ( $8.595 \text{ m}^2 \cdot \text{Pa/W}$ ), while that of the other assemblies ( $8.685\text{--}12.015 \text{ m}^2 \cdot \text{Pa/W}$ ) was higher than that of the sum of the corresponding samples ( $8.675\text{--}8.795 \text{ m}^2 \cdot \text{Pa/W}$ ). Fick's law is widely applied to describe gas diffusion through a porous medium,  $J = -D_{\text{eff}} \nabla C$ , where  $J$  is the diffusive flux,  $D_{\text{eff}}$  is the effective diffusivity, and  $\nabla C$  is the concentration gradient (Mao and Russell 2008). Fick's law phenomenologically states the relationship between the average flux and the concentration gradient; the effective diffusivity tensor  $D_{\text{eff}}$  characterizes the complex interactions between diffusive molecules and solid media. Therefore, the nonwoven fabric at the top surface of the assembly can be manipulated to a higher concentration gradient than that at the bottom surface of the assembly.

The maximum increase of 193.7% was found in the assembly for the sample “n(60)+s” under the downward condition compared with the spacer, while the minimum increase was 20.44% for the sample “n(30)+s” under the upward condition. The high moisture content in the assembly could reduce the thermal resistance and impact thermal properties. Therefore, a higher evaporation resistance can result in condensation in a multilayer clothing system (Das 2012; Sun et al. 2013; Sinclair, 2014; Mazzuchetti, 2007).

The estimated equations of evaporation resistance values are as defined in Equations 10 and 11 with an adjusted R square at 0.92 and 0.53, corresponding to the two test conditions.

$$\begin{aligned} \text{Evaporation resistance of assembly}_{\text{down}} = & -10.013 + 0.368 \times \text{mass of non-woven} + \\ & 188.955 \times \text{mean pore size, Adjusted } R^2 = 0.92 \end{aligned} \quad (10)$$

$$\begin{aligned} \text{Evaporation resistance of assembly}_{\text{up}} = & 2.678 + 0.14 \times \text{mass of non-woven} \\ & + 16.074 \times \text{mean pore size Adjusted } R^2 = 0.53 \end{aligned} \quad (11)$$

### **Water vapor transmission rate**

The results of the water vapor transmission rate are illustrated in Figure 5(F). The spacer had a much higher value than the other assemblies but was lower than nonwoven fabric. Moreover, there was no difference when testing spacer fabric with the two approaches. However, the assemblies tested upward had 21.03–49.43% higher water vapor transmission than those tested downward. The water vapor transmission of the nonwoven fabric declined from  $0.451$  to  $0.426 \text{ g/m}^2 \cdot 24 \text{ h}$  with a 5.5% reduction from  $30 \text{ g/m}^2$  to  $60 \text{ g/m}^2$ .

The estimated equations of water evaporation transmission values are as defined in Equations 12 and 13 with adjusted R square at 0.867 and 0.9993 corresponding to the two test conditions.

$$\begin{aligned} \text{Water evaporation transmission of assembly}_{\text{down}} = & 0.327 - 0.003 \times \text{mass of non-woven} - 1.481 \\ & \times \text{mean pore size, Adjusted, } R^2 = 0.867 \end{aligned} \quad (12)$$

$$\begin{aligned} \text{Water evaporation of assembly}_{\text{up}} = & 0.322 - 0.002 \times \text{thickness of non} \\ & \text{-woven} - 1.138 \times \text{mean pore size, Adjusted } R^2 = 0.9993 \end{aligned} \quad (13)$$

### **Water vapor permeability polyester warp-knitted spacer, cotton nonwoven fabric, and assembly under different air temperatures and humidity**

As depicted in Figure 6, the water vapor permeability of the spacer decreased from  $3,757.51$  to  $812.96 \text{ g/m}^2 \cdot 24 \text{ h}$ , and the total reduction was 78.3% when air temperature and humidity varied from  $25^\circ$  and 45% to  $15^\circ$  and 85%. With increasing humidity and decreasing temperature, water vapor evaporation decreased. The evaporation rate was highest for fabric tested at  $25^\circ$  and 45%. The second-highest value was recorded at  $25^\circ$  and 65%.

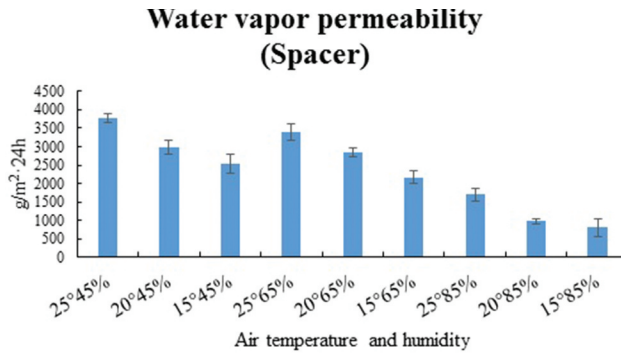


**Figure 6.** Water vapor permeability of the spacer under different air temperature (25°, 20° and 15°) and humidity (45%, 65% and 85%).

$$\text{Water vapor permeability of spacer} = 924.681 + 67.79 \times \text{Temperature} + 9.857 \times \text{humidity} + 1465.012 \times \text{Large pore size}, \text{ Adjusted } R^2 = 1 \quad (14)$$

As depicted in Figure 7, the water vapor permeability of the nonwoven fabrics decreased from 759.05 to 206.82 g/m²·24 h for fabric with 30 g/m², 680.9 to 221.29 g/m²·24 h for fabric with 40 g/m², 643.24 to 180.68 g/m²·24 h for fabric with 50 g/m², and 599.72 to 161.86 g/m²·24 h for fabric with 60 g/m². The total reduction was 78.3% when air temperature and humidity varied from 25° and 45% to 15° and 85%.

$$\text{Water vapor permeability of non woven} = 510.137 + 15.867 \times \text{Temperature} - 3.415 \times \text{humidity} + 12.614 \times \text{Large pore size}, \text{ Adjusted } R^2 = 1 \quad (15)$$

As depicted in Figure 8(a), when nonwoven was placed at the bottom of space, the water vapor permeability of the assembly decreased from 1,009.4 to 147.37 g/m²·24 h, and the total reduction was 85.4% when air temperature and humidity varied from 25° and 45% to 15° and 85%. When nonwoven was placed at the top of the space, the water vapor permeability of the assembly decreased from 1,197.84 to 224.47 g/m²·24 h, and the total reduction was 81.2% when air temperature and humidity varied from 25° and 45% to 15° and 85%. Moreover, the values of upward testing were slightly higher than that of downward testing. The differences between the downward and upward tests for each sample ranged from 3.18% to 54.65%.

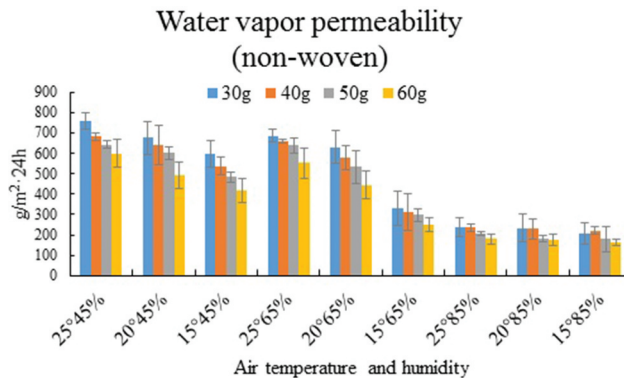


**Figure 7.** Water vapor permeability of non-woven fabric under different air temperature (25°, 20° and 15°) and humidity (45%, 65% and 85%).



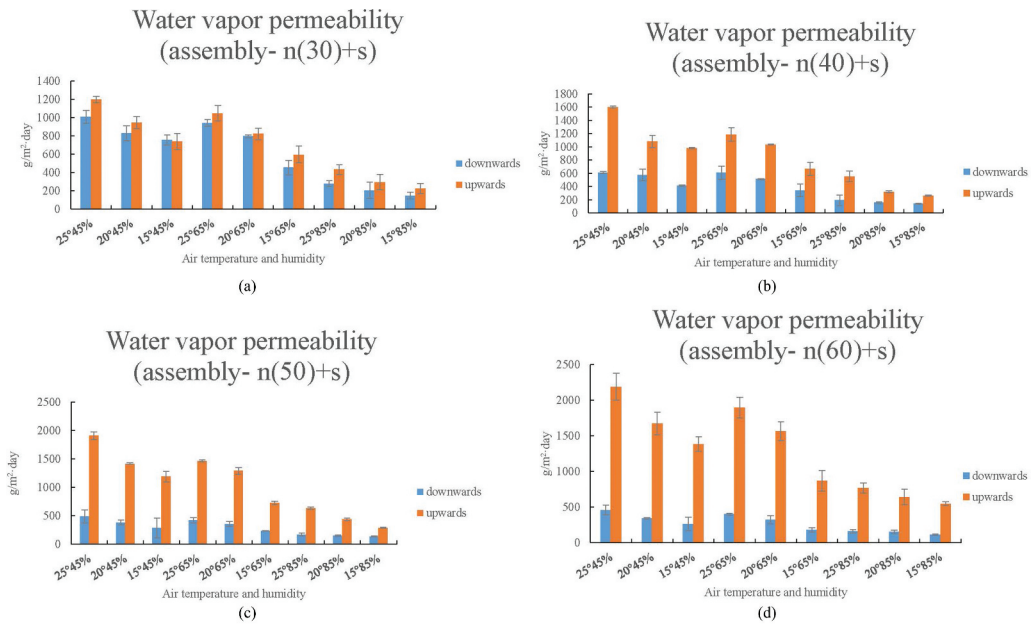


**Figure 8.** Water vapor permeability of assembly of spacer and non-woven fabric under different air temperature (25°, 20° and 15°) and humidity (45%, 65% and 85%) ((a) shows the assembly of spacer and 30 g/m<sup>2</sup> non-woven fabric; (b) shows the assembly of spacer and 40 g/m<sup>2</sup> non-woven fabric.). Water vapor permeability of assembly of spacer and non-woven fabric under different air temperature (25°, 20° and 15°) and humidity (45%, 65% and 85%) ((c) shows the assembly of spacer and 50 g/m<sup>2</sup> non-woven fabric; (d) shows the assembly of spacer and 60 g/m<sup>2</sup> non-woven fabric.).

As depicted in [Figure 8\(b\)](#), when the assembly was tested under the downward condition, the water vapor permeability decreased from 610.25 to 139.57 g/m<sup>2</sup>·24 h, and the total reduction was 77.1% when air temperature and humidity varied. When the assembly was tested under the upward condition, the water vapor permeability decreased from 1,599 to 261.6 g/m<sup>2</sup>·24 h, and the total reduction was 83.6% when air temperature and humidity varied from 25° and 45% to 15° and 85%. Moreover, the values of upward testing were slightly higher than that of downward testing. There were differences between the two types of tests from 87.44% (minimum) to 190.27% (maximum).

As depicted in [Figure 8\(c\)](#), when nonwoven was placed at the bottom of space, the water vapor permeability of the assembly decreased from 489.99 to 137.05 g/m<sup>2</sup>·24 h. In contrast, when nonwoven was placed at the top of the spacer, the water vapor permeability of the assembly decreased from 1,911.73 to 290.6 g/m<sup>2</sup>·24 h. Moreover, the values of upward testing were slightly higher than that of downward testing. The differences ranged from 112.04% to 313.65%.

As depicted in [Figure 8\(d\)](#), when nonwoven was placed at the bottom of space, the water vapor permeability of the assembly decreased from 458.97 to 111.05 g/m<sup>2</sup>·24 h, and the total reduction was 75.8% when air temperature and humidity varied from 25° and 45% to 15° and 85%. When nonwoven was placed at the top of the space, the water vapor permeability of the assembly decreased from 2,191.38 to 546.52 g/m<sup>2</sup>·24 h, and the total reduction was 75.1% when air temperature and humidity varied from 25° and 45% to 15° and 85%. Moreover, the values of upward testing were slightly higher than that of downward testing. The differences increased from 326.53% (lowest) to 427.28% (highest) compared with other assemblies.

With the increase in the mass of the nonwoven fabric, the water vapor permeability decreased during downward testing but increased during upward testing. Hence, the differences under the two test conditions widened. The difference between them increased from 3.18% (minimum) to 427.28% (maximum) because higher airflow occurred through the cross-section of the spacer, accelerating the

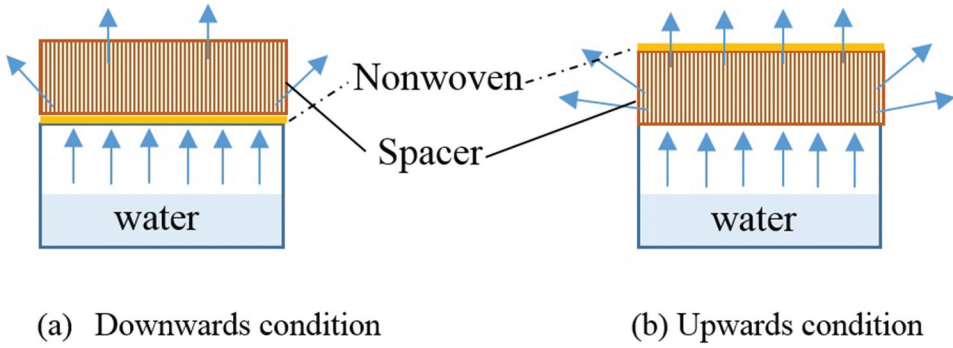


**Figure 9.** the demonstration of water vapor permeability of assembly.

water vapor transport in the transverse and horizontal directions. The mass and thickness of the nonwoven fabric significantly affected the difference between the two testing methods (Figure 9).

The surface fabric of the assembly determined the asymmetric water vapor permeability. Hence, the attachment of nonwoven fabric on the top of the spacer could be an effective solution to achieve the maximum reduction in water vapor permeability of the assembly. In designing a multi-layered system, thinner fabric can be used closer to the skin, while thicker fabric can be used far from the skin to achieve higher thermal resistance and lower evaporation resistance. This is because the total mass transfer ( $g$ ) includes the concentration water vapor diffusion ( $g_f$ ) and convective water vapor diffusion ( $g_m$ ).  $D$  is the mass transfer coefficient,  $l$  is the distance,  $h_m$  is the convective mass transfer coefficient, and  $c$  is the concentration gradient.

$$g = g_f + g_m = \left( \frac{D}{l} + h_m \right) c$$

Under the upward condition, the convective water vapor diffusion was enlarged because of the convection effect within the thicker spacer (thickness of 16 mm). More water vapor can evaporate to air by convection when nonwoven at the top of the spacer than that at the bottom.

The estimated equations of water vapor permeability values are listed in Equations 16 and 17.

$$\text{Water vapor permeability of assembly}_{\text{down}} = 325.827 + 7.978 \times \text{Temperature} + 5.764 \times \text{humidity} + 475.571 \times \text{Large pore size}, \text{Adjusted } R^2 = 1 \quad (16)$$

$$\text{Water vapor permeability of assembly}_{\text{up}} = 299.573 + 38.012 \times \text{Temperature} - 3.403 \times \text{humidity} + 213.308 \times \text{Large pore size}, \text{Adjusted } R^2 = 1 \quad (17)$$

## Conclusions

This study used spacer and nonwoven assembly to improve water vapor permeability and thermal insulation. It was suggested that the cover close to the skin could be a thin fabric, while the cover far from the skin could be thicker. Accordingly, the cotton nonwoven fabric and spacer fabric assembly could provide higher water permeability and a higher thermal insulation ratio. This practical, low-cost solution can improve heat retention and moisture-transfer efficiency and conserve heat energy, implying that the heat transfer efficiencies can be improved using a specific combination of different spacers and nonwoven fabrics. The enhanced assembly performance is likely caused by the combined effect of heat and moisture-transfer mechanisms.

## Highlights

- We investigated the thermal properties and water vapor permeability of assembly-combined thicker spacer (16 mm) and various cotton non-woven fabrics.
- The asymmetric heat- and moisture-transfer properties of porous assembly were found.
- It recommended that lighter or thinner fabric should be used closer to the skin, and heavier and thicker fabric should be used far from the skin to achieve higher thermal resistance and lower evaporation resistance

## Acknowledgements

This work was supported by the Natural Science Foundation of Shanghai (21ZR1400100), Fundamental Research Funds for the Central University (2232020 D-45 and 2232020E-06), by Shanghai Style fashion design and value creation knowledge service center (ZX201311000031).

## Disclosure statement

No potential conflict of interest was reported by the author(s).

## Funding

The work was supported by the Natural Science Foundation of Shanghai [21ZR1400100]; Innovation and Technology Fund of Hong Kong [ITS/315/21]; Environment and Conservation Fund [91/2021]; PolyU Endowed Young Scholars Scheme [84cc]; Research Grants Council of the Hong Kong Special Administrative Region, China [Project No.: PolyU 252029/19E; PolyU 152052/21E]; Fundamental Research Funds for the Central Universities [2232020 D-45 and 2232020 E-06]

## References

- Arumugam, V., R. Mishra, J. Militky, L. Davies, and S. Slater. 2018. Thermal and water vapor transmission through porous warp knitted 3D spacer fabrics for car upholstery applications. *The Journal of the Textile Institute* 109 (3):345–57. doi:10.1080/00405000.2017.1347023.
- Chen, C., Z. Du, W. Yu, and T. Dias. 2018. Analysis of physical properties and structure design of weft-knitted spacer fabric with high porosity. *Textile Research Journal* 88 (1):59–68. doi:10.1177/0040517516676060.
- Chen, Q., D. Shou, R. Zheng, K. P. M. Tang, B. Fu, X. Zhang, and P. Ma. 2021. Moisture and thermal transport properties of different polyester warp-knitted spacer fabric for protective application. *AUTEX Research Journal* 21 (2):182–91. doi:10.2478/aut-2020-0013.
- Das, A. S. 2012. Study on heat and moisture vapor transmission characteristics through multilayered fabric ensembles. *Fibers and Polymers* 13:522–28. doi:10.1007/s12221-012-0522-0.
- Das, A., R. Alagirusamy, K. Shabaridharan, and P. Kumar. 2012. Study on heat transmission through multilayer clothing assemblies under different convective modes. *The Journal of the Textile Institute* 103:777–86. doi:10.1080/00405000.2011.607570.
- Eom, R., H. Lee, and Y. Lee. 2019. Evaluation of Thermal Properties of 3D Spacer Technical Materials in Cold Environments using 3D Printing Technology. *Polymers* 11 (9):1438. doi:10.3390/polym11091438.
- Ertekin, G., and A. Marmarali. 2011. Heat, air and water vapor transfer properties of circular knitting spacer fabrics. *Tekstil ve Konfeksiyon* 21 (4):369–73.
- Ghorbani, V., A. A. A. Jeddi, H. Dabiryan, and A. A. Ramezaniapour. 2020. Investigation of the flexural behavior of self-consolidating mortars reinforced with net warp-knitted spacer fabrics. *Construction and Building Materials* 232 (30):117270. doi:10.1016/j.conbuildmat.2019.117270.
- Gozde, E. 2017. Analysis of thermos-physiological comfort and moisture management properties of flat knitted spacer fabrics. *Tekstil ve Konfeksiyon* 27 (3):241–50.
- Jia, H., J. Zhu, D. Dereje, Z. Li, and J. Guo. 2018. Solar thermal energy harvesting properties of spacer fabric composite used for transparent insulation materials. *Solar Energy Materials and Solar Cells* 174:140–45. doi:10.1016/j.solmat.2017.08.039.
- Krumm, D., S. Schwanitz, and S. Odenwald. 2020. Seat cushions made of warp knitted spacer fabrics influence seat transmissibility. *Applied Ergonomics* 86. doi:10.1016/j.apergo.2020.103099.

- Lo, W., D. Wong, K. Yick, S. Ng, and J. Yip. 2018. The biomechanical effects and perceived comfort of textile-fabricated insoles during straight line walking. *Prosthetics and Orthotics International* 42 (2):153–62. doi:[10.1177/0309364617696084](https://doi.org/10.1177/0309364617696084).
- Mao, N., and S. J. Russell. 2007. The Thermal Insulation Properties of Spacer Fabrics with a Mechanically Integrated Wool Fiber Surface. *Textile Research Journal* 77 (12):914–22. doi:[10.1177/0040517507083524](https://doi.org/10.1177/0040517507083524).
- Mazzuchetti, G., G. Lopardo, and R. Demichelis. 2007. Influence of nonwoven fabrics' physical parameters on thermal and water vapor resistance. *Journal of Industrial Textiles* 36 (3):253–64. doi:[10.1177/1528083707072366](https://doi.org/10.1177/1528083707072366).
- Morrissey, M. P., and R. M. Rossi. 2015. The effect of metallisation, porosity and thickness on the thermal resistance of two-layer fabric assemblies. *Journal of Industrial Textiles* 44 (6):912–23. doi:[10.1177/1528083713519665](https://doi.org/10.1177/1528083713519665).
- Onal, L., and M. Yildirim. 2012. Comfort properties of functional three-dimensional knitted spacer fabrics for home-textile applications. *Textile Research Journal* 82 (17):1751–64. doi:[10.1177/0040517512444331](https://doi.org/10.1177/0040517512444331).
- Ozer, S., Y. Yuksel, and Y. Korkmaz. 2020. Evaluation of compression-recovery and thermal characteristics of multilayer bedding textiles. *International Journal of Clothing Science and Technology* 32 (5):631–43. doi:[10.1108/IJCST-04-2019-0054](https://doi.org/10.1108/IJCST-04-2019-0054).
- Rajan, T. P., L. D. Souza, G. Ramakrishnan, P. Kandhavadvu, and C. Vigneswaran. 2016. Influence of porosity on water vapor permeability behavior of warp knitted polyester spacer fabrics. *Journal of Industrial Textiles* 45 (5):796–812. doi:[10.1177/1528083714540697](https://doi.org/10.1177/1528083714540697).
- Rajan, T. P., and S. Sundaresan. 2020. Thermal comfort properties of plasma-treated warp-knitted spacer fabric for the shoe insole. *Journal of Industrial Textiles* 49 (9):1218–32. doi:[10.1177/1528083718811084](https://doi.org/10.1177/1528083718811084).
- Shou, D., J. Fan, and F. Ding. 2010. A difference-fractal model for the permeability of fibrous porous media. *Physics Letters A* 374 (10):1201–04. doi:[10.1016/j.physleta.2010.01.002](https://doi.org/10.1016/j.physleta.2010.01.002).
- Shou, D., J. Fan, M. Mei, and F. Ding. 2014. An analytical model for gas diffusion through nanoscale and microscale fibrous media. *Microfluidics and Nanofluidics* 16 (1–2):381–89. doi:[10.1007/s10404-013-1215-8](https://doi.org/10.1007/s10404-013-1215-8).
- Sinclair, R. 2014. *Textiles and Fashion Materials, Design and Technology*, 739–61. Woodhead Publishing Series in Textiles.
- Sun, C., J. Fan, H. Wu, Y. Wu, and X. Wan. 2013. Cold protective clothing with reflective nano-fibrous interlayers for improved comfort. *International Journal of Clothing Science and Technology* 25 (5):380–88. doi:[10.1108/IJCST-06-2012-0034](https://doi.org/10.1108/IJCST-06-2012-0034).
- Tang, K. P. M., Y. Wu, and J. Fan. 2020. Effect of material property, surface temperature and contact duration on the thermal sensation when contacting shell materials of electronic devices. *Applied Ergonomics* 86:103104. doi:[10.1016/J.APERGO.2020.103104](https://doi.org/10.1016/J.APERGO.2020.103104).
- Veerakumar, A., M. Rajesh, M. Jiri, and J. Salacova. 2017. Investigation on thermo-physiological and compression characteristics of weft-knitted 3D spacer fabrics. *The Journal of the Textile Institute* 108 (7):1095–105. doi:[10.1080/00405000.2016.1220035](https://doi.org/10.1080/00405000.2016.1220035).
- Wang, F., D. Wei, Y. Li, T. Chen, P. Mu, H. Sun, Z. Zhu, W. Liang, and A. Li. 2019. Chitosan/Reduced graphene oxide-modified spacer fabric as a salt-resistant solar absorber for efficient solar steam generation. *Journal of Materials Chemistry A* 7 (31):18311–17. doi:[10.1039/C9TA05859A](https://doi.org/10.1039/C9TA05859A).
- Xu, X., T. P. Rioux, N. Pomerantz, and S. Tew. 2019. Effects of fabric on thermal and evaporative resistances of chemical protective ensembles: Measurement and quantification. *Measurement* 136:248–55. doi:[10.1016/j.measurement.2018.12.078](https://doi.org/10.1016/j.measurement.2018.12.078).
- Yip, J., and S. Ng. 2009. Study of three-dimensional spacer fabrics: Molding properties for intimate apparel application. *Journal of Materials Processing Technology* 209 (1):58–62. doi:[10.1016/j.jmatprotec.2008.01.029](https://doi.org/10.1016/j.jmatprotec.2008.01.029).
- Yoo, S., and E. Kim. 2008. Effects of Multilayer Clothing System Array on Water Vapor Transfer and Condensation in Cold Weather Clothing Ensemble. *Textile Research Journal* 78 (3):189–97. doi:[10.1177/0040517507078793](https://doi.org/10.1177/0040517507078793).
- Zhu, M., Y. Huang, W. Ng, J. Liu, Z. Wang, Z. Wang, H. Hu, and C. Zhi. 2016. 3D spacer fabric based multifunctional triboelectric nanogenerator with great feasibility for mechanized large-scale production. *Nano Energy* 27:439–46. doi:[10.1016/j.nanoen.2016.07.016](https://doi.org/10.1016/j.nanoen.2016.07.016).
- Ziaei, M., and M. Ghane. 2013. Thermal insulation property of spacer fabrics integrated by ceramic powder impregnated fabrics. *Journal of Industrial Textiles* 43 (1):20–33. doi:[10.1177/1528083712446384](https://doi.org/10.1177/1528083712446384).